



HAL
open science

Effective diffusivity of microswimmers in a crowded environment

Marvin Brun-Cosme-Bruny, Eric Bertin, Benoit Coasne, Philippe Peyla,
Salima Rafai

► **To cite this version:**

Marvin Brun-Cosme-Bruny, Eric Bertin, Benoit Coasne, Philippe Peyla, Salima Rafai. Effective diffusivity of microswimmers in a crowded environment. *The Journal of Chemical Physics*, 2019, 10.1063/1.5081507 . hal-01923729v1

HAL Id: hal-01923729

<https://hal.science/hal-01923729v1>

Submitted on 15 Nov 2018 (v1), last revised 15 Sep 2020 (v2)

HAL is a multi-disciplinary open access archive for the deposit and dissemination of scientific research documents, whether they are published or not. The documents may come from teaching and research institutions in France or abroad, or from public or private research centers.

L'archive ouverte pluridisciplinaire **HAL**, est destinée au dépôt et à la diffusion de documents scientifiques de niveau recherche, publiés ou non, émanant des établissements d'enseignement et de recherche français ou étrangers, des laboratoires publics ou privés.

Effective diffusivity of microswimmers in a crowded environment

Marvin Brun-Cosme-Bruny,¹ Eric Bertin,¹ Benoît Coasne,¹ Philippe Peyla,¹ and Salima Rafai^{1, *}

¹*Univ. Grenoble Alpes, CNRS, LIPhy, F-38000 Grenoble, France*

(Dated: November 15, 2018)

The microalga *Chlamydomonas Reinhardtii* (CR) is used here as a model system to study the effect of complex environments on the swimming of micro-organisms. Its motion can be modelled by a run and tumble mechanism so that it describes a persistent random walk from which we can extract an effective diffusion coefficient for the large-time dynamics. In our experiments, the complex medium consists in a series of pillars that are designed in a regular lattice using soft lithography microfabrication. The cells are then introduced in the lattice, and their trajectories within the pillars are tracked and analyzed. The effect of the complex medium on the swimming behaviour of microswimmers is analyzed through the measure of relevant statistical observables. In particular, the mean correlation time of direction and the effective diffusion coefficient are shown to decrease when increasing the density of pillars. This provides some bases of understanding for active matter in complex environments.

I. INTRODUCTION

Self-propelled particles represent an out-of-equilibrium system of great interest for a large community of physicists [1]. The dynamics of most microswimmers, natural or artificial, perform a “run and tumble” dynamics of swimming [2]. This terminology, initially dedicated to *E-coli* bacteria, describes an alternation of directed motion at a given velocity - the runs - and reorientation of the direction - the tumbles. Other dynamics of swimming consist in Active Brownian particles where the direction angle changes continuously in a diffusive manner [3]. These modes of swimming have been shown to be crucial in the search of chemicals or nutrients [4]. Depending on systems, the decorrelation of direction emerges from different mechanisms. In bacteria, tumbles are due to the unbundling of flagella [5], in the microalga *Chlamydomonas Reinhardtii*, tumbles have been shown to be due to asynchronous periods of beating [6]. In artificially built microswimmers such as Janus particles, thermal rotational Brownian motion is usually responsible for the randomisation of orientation [7, 8]. Most of the time, the swimming dynamics can be fairly described as a persistent random walk.

Hence, considering large enough time scales, microswimmers explore their environment in a diffusive-like manner. A nonequilibrium statistical physics framework can then be built in order to deeper understand the behavior of active matter [9]. To predict active matter behaviour in realistic conditions such as crowded living tissues, suspensions of cells or porous media, there is a major need to understand the interaction of self-propelled par-

ticles with a complex environment [10].

In this work, we quantify experimentally the swimming dynamics of a natural microswimmer – *Chlamydomonas Reinhardtii* – within a micropatterned environment. We show that the effective diffusivity of microswimmers is hindered by the presence of obstacles, and that the distribution of swimming directions is no longer isotropic. In addition, a theoretical modeling in terms of an effective anisotropic scattering medium allows us to relate the anisotropy of swimming directions and the decrease of the effective diffusion coefficient.

II. MATERIALS AND METHODS

The green microalga *Chlamydomonas Reinhardtii* (CR) is a biflagellated photosynthetic cell of about 10 μm diameter [11]. Cells are grown under a 14h/10h light/dark cycle at 22 $^{\circ}\text{C}$ and are harvested in the middle of the exponential growth phase. This microalga propels itself in a break-stroke-type swimming using its two front flagella.

CR suspensions are used with no further preparation. Suspensions are dilute enough with a volume fraction of about 0.05%, so that hydrodynamic interactions among the particles are negligible. The cells are then introduced within a complex medium composed of a square lattice of 200 μm -diameter pillars regularly spaced by a surface-to-surface minimal inter-pillar distance d (figure 1). The distance d between the surfaces of the pillars ranges from 20 μm to 50 μm with a 10 μm increment, and from 50 μm to 370 μm with a 40 μm increment. This represents a porosity $\delta = 1 - \pi R^2 / (d + 2R)^2$ ranging from 0.35 to 0.90. Pillars are made of transparent PDMS using soft lithography processes [12]. Their diameter is kept constant to 200 μm . This is of the same order as the persistence length of the swimming

* salima.rafai@univ-grenoble-alpes.fr

dynamics of the cells ($\sim 180\mu\text{m}$). The height of the pillars is $70\mu\text{m}$, which represents about 7 cell diameters. Our control parameter is d , which controls the density of the complex medium that the cells experience.

The observations are made by means of bright field microscopy. The chamber is observed under an inverted microscope (Olympus IX71) coupled to a CMOS camera (Imaging Source) used at a frame rate of 15 frames per second. A low magnification objective ($\times 1.25$) provides a wide field of view of $800\mu\text{m} \times 800\mu\text{m}$ as well as a large depth of field. The sample is enclosed in an occulting box with two red filtered windows for visualisation. The red filters prevent any parasite light that could trigger phototaxis (*i.e.* a biased swimming toward a light source) [11, 13].

Particle tracking is performed using Trackpy [14], a Python library based on Crocker and Grier's algorithm [15]. Relevant quantities such as the mean square displacements (MSD) and the correlation functions of directions are then extracted from an ensemble average performed over long lasting movies (6 min).

Figure 1 shows the typical geometry and a set of trajectories of cells measured over 10 seconds for a given inter-pillar distance of 50 micrometers ($d = 50\mu\text{m}$) at a time interval of $1/15\text{ s}$.

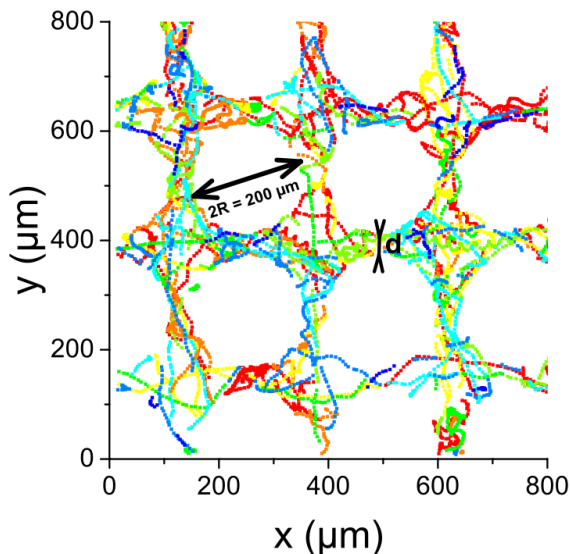


FIG. 1. Map of trajectories tracked over 10 seconds within a square lattice of pillars with $d = 50\mu\text{m}$ at a time interval of $1/15\text{ s}$. The color is mapped on the particle index.

III. RESULTS

A. Anisotropy

The first noticeable effect of the lattice of obstacles onto the cells is an anisotropy of their swimming directions. The squared lattice of pillars constrains the trajectories of microswimmers to a set of privileged (x, y) directions as shown from the orientation distribution plotted in figure 2. Here, we define the orientations as the mean orientation of the trajectory over 1 s. While orientations of microswimmers are isotropically distributed in a free medium ($d \rightarrow \infty$), the distributions show peaks around $\pi/2(\text{mod } \pi/2)$ when cells are placed within the complex medium. This clearly demonstrates the privileged directions taken by microswimmers. This reflects that, most of the time, the pillars orient the swimming along corridors between pillars. This effect becomes more and more pronounced as d is decreased.

To try to better understand these results, we introduce a relatively simple theoretical model consisting of an active Brownian particle immersed in an effective anisotropic scattering medium. The active Brownian particle is characterized by its position \mathbf{r} (in 2D) and an angle θ defining its direction of motion. The particle moves at a constant speed v_0 . In the absence of obstacles, the angle θ has a purely diffusive dynamics:

$$\dot{\mathbf{r}} = v_0 \mathbf{e}(\theta), \quad \dot{\theta} = \xi(t) \quad (1)$$

where $\xi(t)$ is a white noise satisfying $\langle \xi(t) \rangle = 0$ and

$$\langle \xi(t) \xi(t') \rangle = 2D_R \delta(t - t'). \quad (2)$$

The angular diffusion coefficient is related to the persistence time τ by $\tau = 1/D_R$. To make the full problem tractable, the lattice of pillars is modeled as an effective anisotropic scattering medium, with a probability rate

$$\lambda(\theta) = \lambda_0 - \lambda_4 \cos(4\theta). \quad (3)$$

The two parameters λ_0 and λ_4 are constrained by $|\lambda_4| \leq \lambda_0$. After scattering, the new angle θ' is randomly chosen from a uniform distribution. The model thus boils down to a combination of the active Brownian particle and the run-and-tumble model, with here an anisotropic tumbling rate. Technical details are reported in Appendix A. Using some standard approximation techniques, we eventually obtain the spatially averaged probability distribution $\overline{P}(\theta)$ of swimming directions θ

$$\overline{P}(\theta) = \frac{1}{2\pi} \left(1 + \frac{\lambda_4}{16D_R + \lambda_0} \cos(4\theta) \right). \quad (4)$$

We use this form to fit the experimental data, under the assumption $\lambda_0 = \lambda_4 = \lambda$ (which means that particles can travel freely when their direction is aligned either with the x or y axis). This fitting procedure thus allows us to determine the experimental values of λ .

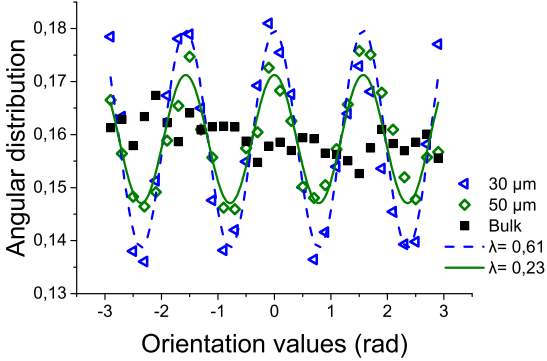


FIG. 2. Orientation distributions of *Chlamydomonas runs* for different interpillar distances d . To do so, the orientation is measured over 1 s. These distributions are fitted with Eq. (4), assuming $\lambda_0 = \lambda_4 = \lambda$.

B. Mean square displacements and correlations

From the measured trajectories, we evaluate and plot in figure 3-a the mean square displacement (MSD) $\langle \mathbf{r}^2(t) \rangle$ for different values of d ranging from 20 to 370 μm . In a free medium (*i.e.* without pillars), the swimming of CR has been shown to be well characterized by a persistent random walk [6, 16, 17] in absence of tropism. Hence, the behaviour of microswimmers can be modelled as a ballistic motion at short timescales (below ~ 1 s) and a diffusive-like one at longer timescales. Here, we assume that the MSD in the presence of obstacles can still be described by a persistent random walk and we fit the curves in figure 3 with the following semi-empirical equation:

$$\langle \mathbf{r}^2(t) \rangle = 4D_{\text{eff}}t - 2D_{\text{eff}}t_{\text{eff}} \left[1 - \exp\left(\frac{-2t}{t_{\text{eff}}}\right) \right] \quad (5)$$

where t_{eff} is the effective correlation time and L_{eff} the effective persistence length of the swimming. In a free medium ($d \rightarrow \infty$), we denote by t_0 and L_0 the correlation time and persistence length respectively. Experimental measurements give $t_0 = 2.7$ s and $L_0 = 180 \mu\text{m}$

In addition, we characterize independently the persistence time by measuring the correlation func-

tion of direction defined as

$$C(t) = \langle \mathbf{k}(t_0) \cdot \mathbf{k}(t_0 + t) \rangle,$$

where $\langle \dots \rangle$ denotes an average over time t_0 and over all tracked trajectories and \mathbf{k} a unit vector along the trajectory (Figure 3-b). Correlations with infinite decay time ($C(t) = 1$ for all $t > 0$) correspond to swimming directions preserved over arbitrarily long times characteristic of a purely ballistic regime; in contrast, a zero life-time ($C(t) = 0$ for all $t > 0$) corresponds to the standard random walk behaviour (analogous to Brownian motion). The measured correlation functions show two characteristic times: the first one corresponds to an helical shape [18] of the trajectory and the second one t_{eff} represents the mean time of persistence over which the swimming direction is preserved. The extracted characteristic time t_{eff} allows one to constraint the fitting procedure of equation (5) and to evaluate L_{eff} for different values of d .

C. Diffusive regime

The long timescales dynamics can be then described by a diffusive-like behaviour. From the measured MSD and the correlation function of direction, we similarly obtain the effective diffusivity D_{eff} as a function of d/L_0 .

Figure 4 shows the experimentally measured effective diffusion coefficient D_{eff} of microswimmers within the lattice, normalized by the bulk diffusion coefficient D_0 . These results are compared with the theoretical prediction (see Appendix A)

$$\frac{D}{D_0} = \frac{1 + \frac{\tilde{\lambda}_4^2}{4(9+\tilde{\lambda}_0)(16+\tilde{\lambda}_0)}}{(1 + \tilde{\lambda}_0) \left(1 - \frac{\tilde{\lambda}_4^2}{4(1+\tilde{\lambda}_0)(9+\tilde{\lambda}_0)} \right)} \quad (6)$$

where the dimensionless parameters

$$\tilde{\lambda}_0 = \frac{\lambda_0}{D_R}, \quad \tilde{\lambda}_4 = \frac{\lambda_4}{D_R} \quad (7)$$

have been defined. Here, as before we have assumed that both parameters are equal, and taken the value of $\lambda_0 = \lambda_4 = \lambda$ obtained from the fit of the distribution of swimming directions (fig. 2). This assumption might break down at low inter-pillar distances. The value of the angular diffusion coefficient corresponding to $1/t_0$ is taken as $D_R = 0.37 \text{ s}^{-1}$.

IV. CONCLUSION

In this paper, we show that the diffusivity of puller-type microswimmers (here *Chlamydomonas*

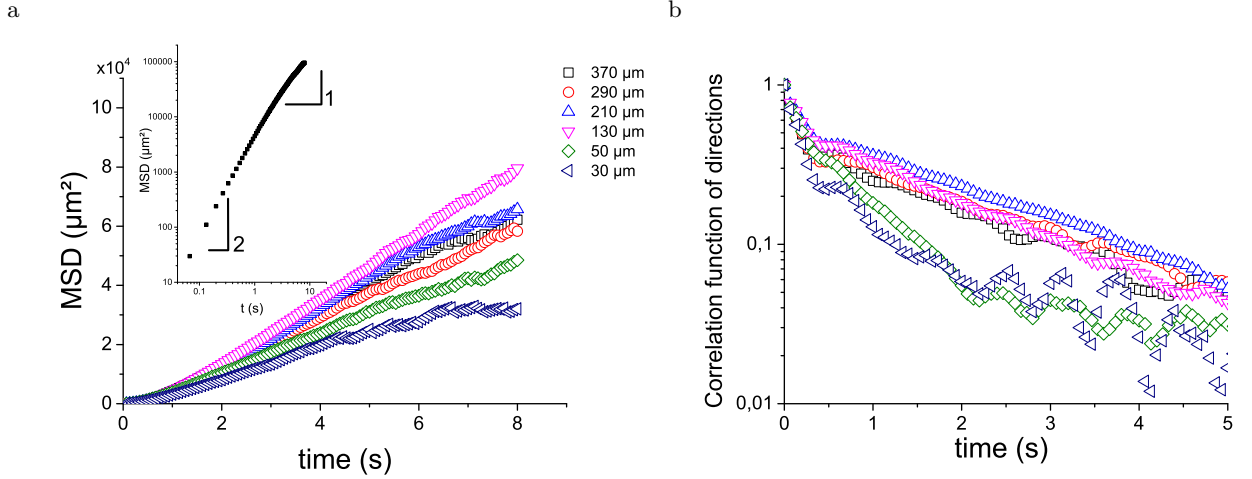


FIG. 3. a. Mean square displacements for several interpillar distances d . The inset shows the two limiting cases: a slope of 2 in $\log - \log$ representation followed by a linear regime at longer timescales. b. Correlation function of direction as a function of time for different values of d .

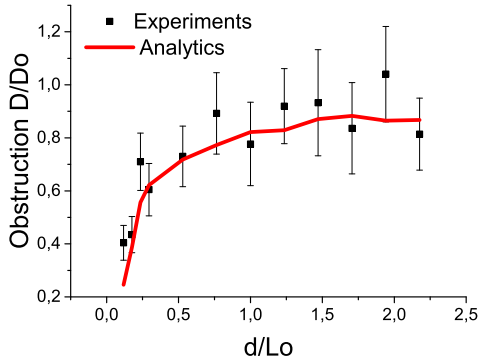


FIG. 4. Normalized effective diffusion coefficient D_{eff} as a function of the interpillar distance d . The bulk diffusion, used for normalization, is $D_0 = 3000 \mu\text{m}^2/\text{s}$. The continuous line represents the prediction of Eq. (6), with λ fitted from Eq. (4).

Reinhardtii) is strongly affected when embedded in a complex medium (here a pillar lattice). We show that geometrical constraints are sufficient to provide a good understanding of the diffusivity as a function of the pillar density. Hydrodynamic interactions can be ignored, at least at low volume fractions of microswimmers. This seems to favour the hypothesis that only steric interactions drive the coupling between pullers and walls [19] rather than the hydrodynamic hypothesis [20–22].

This paves the way to future studies on behaviours of microswimmers hindered by complex geometrical environments.

Appendix A: Derivation of an effective diffusive description

In this appendix, we provide an approximate statistical description of the effective large scale diffusion of swimmers, under some simplifying assumptions. The spatially averaged angular distribution of swimmers is also obtained.

We consider a set of active Brownian particles moving in a crowded environment. Assuming that particles do not interact with each other, we can focus on the description of a single particle. The particle is characterized by its position \mathbf{r} (in 2D) and an angle θ defining its direction of motion. The particle moves at a constant speed v_0 . In the absence of obstacles, the angle θ has a purely diffusive dynamics, and the model is described by Eqs. (1) and (2). To introduce the pillars in a simplified way so that the problem remains analytically tractable, we use an effective medium approach. As a first approximation, the effect of pillars is to generate random changes in the direction of motion of the swimmers. To simplify the problem, we neglect spatial correlations and simply retain as a key ingredient the 4-fold anisotropy resulting from the lattice of pillars. We then describe the crowded environment by a stochastic probability $\lambda(\theta)$ to change direction after collision with a pillar. As for run-and-tumble particles, we assume that the new direction θ' is chosen in a uniform way. Doing so, we neglect the probable anticorrelation between θ and θ' (one expects that the swimmer is more likely to go backward after a collision with a pillar, but this effect is probably not very strong).

The anisotropy of the medium is kept in the description through the θ dependence of the ‘tumbling’ rate $\lambda(\theta)$, and we choose as the simplest description to keep only the zeroth and fourth angular mode, leading to

$$\lambda(\theta) = \lambda_0 - \lambda_4 \cos(4\theta). \quad (\text{A1})^{260}$$

The positivity of $\lambda(\theta)$ implies that $\lambda_0 > 0$ and $|\lambda_4| \leq \lambda_0$. In the experiment, the arrangement of pillars corresponds to an effective medium that is less crowded along the x and y axes than along the diagonal directions. We have chosen the sign convention in Eq. (A1) so that the experimental situation corresponds to $\lambda_4 > 0$.

Effective diffusion equation ²⁷⁰

The probability density $P(\mathbf{r}, \theta)$ to find the swimmer at position \mathbf{r} with velocity angle θ obeys the following dynamics:

$$\begin{aligned} \partial_t P(\mathbf{r}, \theta) + \nabla \cdot [v_0 \mathbf{e}(\theta) P(\mathbf{r}, \theta)] &= D_R \partial_\theta^2 P(\mathbf{r}, \theta) \\ -\lambda(\theta) P(\mathbf{r}, \theta) + \frac{1}{2\pi} \int d\theta' \lambda(\theta') P(\mathbf{r}, \theta') & \quad (\text{A2}) \end{aligned}$$

We define the angular Fourier expansion of the distribution $P(\mathbf{r}, \theta)$,

$$P(\mathbf{r}, \theta) = \frac{1}{2\pi} \sum_{k=-\infty}^{\infty} f_k(\mathbf{r}) e^{-ik\theta} \quad (\text{A3})$$

$$f_k(\mathbf{r}) = \int_{-\pi}^{\pi} d\theta P(\mathbf{r}, \theta) e^{ik\theta} \quad (\text{A4})$$

Note that $\rho(\mathbf{r}) \equiv f_0(\mathbf{r})$ is simply the density field. Expanding Eq. (A2) in angular Fourier modes, we get

$$\begin{aligned} \partial_t f_k + \frac{v_0}{2} (\hat{\nabla} f_{k-1} + \hat{\nabla}^* f_{k+1}) &= -D_R k^2 f_k \\ -\lambda_0 f_k + \frac{\lambda_4}{2} (f_{k+4} + f_{k-4}) \\ + \delta_{k,0} \left[\lambda_0 \rho - \frac{\lambda_4}{2} (f_4 + f_4^*) \right] & \quad (\text{A5}) \end{aligned}$$

where the star denotes the complex conjugate, and $\delta_{k,0} = 1$ for $k = 0$ and 0 otherwise. The notations $\hat{\nabla}$ and $\hat{\nabla}^*$ denote the complex differential operator

$$\hat{\nabla} = \partial_x + i\partial_y, \quad \hat{\nabla}^* = \partial_x - i\partial_y, \quad (\text{A6})$$

with $i^2 = -1$. For $k = 0$, Eq. (A5) simply yields a continuity equation

$$\partial_t \rho + \frac{v_0}{2} \text{Re}(\hat{\nabla}^* f_1) = 0 \quad (\text{A7})$$

which is equivalent to the standard continuity equation

$$\partial_t \rho + \nabla \cdot (\rho \mathbf{v}) = 0, \quad (\text{A8})$$

where \mathbf{v} is the hydrodynamic velocity field, with $\rho \mathbf{v} = v_0(\text{Re}f_1, \text{Im}f_1)$. The goal of the following study is to obtain a closed expression of the field f_1 in terms of the density field ρ and its derivatives, thus turning Eq. (A7) into a closed differential equation on the field ρ . To express f_1 as a function of ρ and its derivatives, we need to rely on Eq. (A5), which corresponds to an infinite hierarchy of coupled equations. To make the problem tractable, we need to truncate this hierarchy. Because of the 4-fold symmetry of the problem, we need to keep angular modes at least up to f_4 . In what follows, we neglect all modes f_k with $|k| > 4$. For $k \neq 0$, the dynamics of f_k involves a relaxation term $-(D_R k^2 + \lambda_0)f_k$, while the density field does not have such a relaxation dynamics. Hence the density field ρ is a ‘slow’ variable, while the fields $f_{k \neq 0}$ are ‘fast’ variables. As a result, on time scales larger than $1/D_R$, the time derivatives $\partial_t f_k$ can be neglected for $k \neq 0$. We end up with the following set of equations

$$f_1 = -a_1 (\hat{\nabla} \rho + \hat{\nabla}^* f_2) + b_1 f_3^* \quad (\text{A9})$$

$$f_2 = -a_2 (\hat{\nabla} f_1 + \hat{\nabla}^* f_3) + b_2 f_2^* \quad (\text{A10})$$

$$f_3 = -a_3 (\hat{\nabla} f_2 + \hat{\nabla}^* f_4) + b_3 f_1^* \quad (\text{A11})$$

$$f_4 = -a_4 \hat{\nabla} f_3 + b_4 \rho \quad (\text{A12})$$

where the coefficients are given by

$$a_k = \frac{v_0}{2(k^2 D_R + \lambda_0)}, \quad b_k = \frac{\lambda_4}{2(k^2 D_R + \lambda_0)}. \quad (\text{A13})$$

We wish to determine an effective diffusion equation from Eq. (A7), and thus we need to express f_1 as a function of ρ up to gradient order. Eq. (A9) provides an expression for f_1 in terms of the fields ρ , f_2 and f_3 . We need to determine f_2 to zeroth order in gradient, and f_3 to first order in gradient. Eq. (A10) shows that at zeroth order in gradient, $f_2 = 0$. Then combining Eqs. (A9), (A11) and (A12), we get at first order in gradient

$$f_3 = -\frac{a_3 b_4 + b_3 a_1}{1 - b_1 b_3} \hat{\nabla}^* \rho \quad (\text{A14})$$

and thus from Eq. (A9),

$$f_1 = -\frac{a_1 + a_3 b_1 b_4}{1 - b_1 b_3} \hat{\nabla} \rho \quad (\text{A15})$$

(again to first order in gradients). We thus finally obtain, using Eq. (A7), the diffusion equation

$$\partial_t \rho = D \Delta \rho \quad (\text{A16})$$

with a diffusion coefficient

$$D = \frac{v_0(a_1 + a_3 b_1 b_4)}{1 - b_1 b_3} \quad (\text{A17})$$

In the absence of obstacles, D reduces to the well-known diffusion coefficient of active Brownian particles,

$$D_0 = \frac{v_0^2}{2D_R} \quad (\text{A18})$$

It is convenient to define the dimensionless parameters

$$\tilde{\lambda}_0 = \frac{\lambda_0}{D_R}, \quad \tilde{\lambda}_4 = \frac{\lambda_4}{D_R} \quad (\text{A19})$$

With these notations, the ratio D/D_0 can be explicitly expressed as

$$\frac{D}{D_0} = \frac{1 + \frac{\tilde{\lambda}_4^2}{4(9+\tilde{\lambda}_0)(16+\tilde{\lambda}_0)}}{(1 + \tilde{\lambda}_0) \left(1 - \frac{\tilde{\lambda}_4^2}{4(1+\tilde{\lambda}_0)(9+\tilde{\lambda}_0)}\right)} \quad (\text{A20})$$

Finally, the mean square displacement is given by

$$\langle \mathbf{r}^2(t) \rangle = 4Dt \quad (\text{A21})$$

Spatially averaged angular distribution

To see if the dynamics of the active Brownian particle keeps track, on large scale, of the

anisotropy of the medium, we compute the spatially integrated angular distribution

$$\overline{P}(\theta) = \int d\mathbf{r} P(\mathbf{r}, \theta) \quad (\text{A22})$$

Keeping as above only angular Fourier modes up to $|k| = 4$, we have

$$\overline{P}(\theta) = \frac{1}{2\pi} \sum_{k=-4}^4 \overline{f}_k(\mathbf{r}) e^{-ik\theta}. \quad (\text{A23})$$

Given that the integral over space of space derivative terms is equal to zero, we get from Eqs. (A9), (A10) and (A11),

$$\overline{f}_1 = b_1 \overline{f}_3^*, \quad \overline{f}_2 = b_2 \overline{f}_2^*, \quad \overline{f}_3 = b_3 \overline{f}_1^* \quad (\text{A24})$$

from which it is easy to show that $\overline{f}_1 = \overline{f}_2 = \overline{f}_3 = 0$. In addition, we have from Eq. (A12) that $\overline{f}_4 = b_4 \overline{\rho} = b_4$, because $\int d\mathbf{r} \rho(\mathbf{r}) = 1$ since we have considered a single particle. We eventually get

$$\overline{P}(\theta) = \frac{1}{2\pi} \left(1 + \frac{\lambda_4}{16D_R + \lambda_0} \cos(4\theta)\right). \quad (\text{A25})$$

-
- [1] M. C. Marchetti, J. F. Joanny, S. Ramaswamy, T. B. Liverpool, J. Prost, M. Rao, and R. A. Simha, *Rev. Mod. Phys.* **85**, 1143 (2013).
- [2] H. C. Berg, *Random walks in biology* (Princeton University Press, 1993).
- [3] M. Cates and J. Tailleur, *EPL (Europhysics Letters)* **101**, 20010 (2013).
- [4] J. G. Mitchell, *The American Naturalist* **160**, 727 (2002).
- [5] H. C. Berg, D. A. Brown, *et al.*, *Nature* **239**, 500 (1972).
- [6] M. Polin, I. Tuval, K. Drescher, J. P. Gollub, and R. E. Goldstein, *Science* **325**, 487 (2009).
- [7] J. R. Howse, R. A. L. Jones, A. J. Ryan, T. Gough, R. Vafabakhsh, and R. Golestanian, *Phys. Rev. Lett.* **99**, 048102 (2007).
- [8] J. Palacci, C. Cottin-Bizonne, C. Ybert, and L. Bocquet, *Phys. Rev. Lett.* **105**, 088304 (2010).
- [9] S. Ramaswamy, *Annual Review of Condensed Matter Physics* **1** (2010), 10.1146/annurev-conmatphys-070909-104101.
- [10] C. Bechinger, R. Di Leonardo, H. Löwen, C. Reichardt, G. Volpe, and G. Volpe, *Reviews of Modern Physics* **88**, 045006 (2016).
- [11] E. H. Harris, *The Chlamydomonas sourcebook: introduction to Chlamydomonas and its laboratory use*, Vol. 1 (Academic press, 2009).
- [12] D. Qin, Y. Xia, and G. M. Whitesides, *Nature protocols* **5**, 491 (2010).
- [13] X. Garcia, S. Rafai, and P. Peyla, *Physical review letters* **110**, 138106 (2013).
- [14] D. B. Allan, T. Caswell, N. C. Keim, and C. M. van der Wel, “Trackpy v0.4.1,” (2018).
- [15] J. C. Crocker and D. G. Grier, *Journal of colloid and interface science* **179**, 298 (1996).
- [16] M. Garcia, S. Berti, P. Peyla, and S. Rafai, *Phys. Rev. E* **83**, 035301 (2011).
- [17] E. A. Codling, M. J. Plank, and S. Benhamou, *Journal of the Royal Society Interface* **5**, 813 (2008).
- [18] Not discussed here as this is a 3d feature of the trajectories and our microscopy analysis is a 2d study.
- [19] V. Kantsler, J. Dunkel, M. Polin, and R. E. Goldstein, *Proceedings of the National Academy of Sciences* **110**, 1187 (2013), <http://www.pnas.org/content/110/4/1187.full.pdf>.
- [20] S. E. Spagnolie, G. R. Moreno-Flores, D. Bartolo, and E. Lauga, *Soft Matter* **11**, 3396 (2015).
- [21] M. Contino, E. Lushi, I. Tuval, V. Kantsler, and M. Polin, *Physical Review Letters* **115**, 1 (2015), arXiv:1511.00888.
- [22] M. Mirzakhloo and M.-R. Alam, *Phys. Rev. E* **98**, 012603 (2018).